ARMY RESEARCH LABORATORY

Anisotropic Dislocation Line Energy and Crack Tip Dislocation Nucleation in αRDX

by Lynn B. Munday and Jaroslaw Knap

ARL-TR-6733 **November 2013**

NOTICES

Disclaimers

The findings in this report are not to be construed as an official Department of the Army position unless so designated by other authorized documents.

Citation of manufacturer's or trade names does not constitute an official endorsement or approval of the use thereof.

Destroy this report when it is no longer needed. Do not return it to the originator.

Army Research Laboratory
Aberdeen Proving Ground, MD 21005-5067

ARL-TR-6733 **November 2013**

Anisotropic Dislocation Line Energy and Crack Tip Dislocation Nucleation in αRDX

Lynn B. Munday and Jaroslaw Knap
Computational and Information Sciences Directorate, ARL

REPORT DOCUMENTATION PAGE	Form Approved OMB No. 0704-0188

1. REPORT DATE *(DD-MM-YYYY)*	2. REPORT TYPE	3. DATES COVERED (From - To)
November 2013	Final	2 June 2012

4. TITLE AND SUBTITLE
Anisotropic Dislocation Line Energy and Crack Tip Dislocation Nucleation in αRDX

5a. CONTRACT NUMBER

5b. GRANT NUMBER

5c. PROGRAM ELEMENT NUMBER

6. AUTHOR(S)
Lynn B. Munday and Jaroslaw Knap

5d. PROJECT NUMBER
MSRM-HSAI

5e. TASK NUMBER

5f. WORK UNIT NUMBER

7. PERFORMING ORGANIZATION NAME(S) AND ADDRESS(ES)
U.S. Army Research Laboratory
ATTN: RDRL-CHI-C
Aberdeen Proving Ground, MD 21005-5067

8. PERFORMING ORGANIZATION REPORT NUMBER
ARL-TR-6733

9. SPONSORING/MONITORING AGENCY NAME(S) AND ADDRESS(ES)

10. SPONSOR/MONITOR'S ACRONYM(S)

11. SPONSOR/MONITOR'S REPORT NUMBER(S)

12. DISTRIBUTION/AVAILABILITY STATEMENT
Approved for public release; distribution is unlimited.

13. SUPPLEMENTARY NOTES

14. ABSTRACT
This work reports on the algorithms used to determine the anisotropic and isotropic elastic properties of dislocations and their nucleation from a crack tip. The appendix contains a numerical implementation of these algorithms in Matlab. The algorithms are demonstrated for the the energetic molecular crystal αRDX, which has orthotropic elastic constants. The energy prefactor tensor is determined for several dislocation and crack tip configurations for RDX in order to calculate dislocation nucleation thresholds for different loading scenarios. Anisotropic results are compared to results obtained using isotropic material averages. The case of crack tip shielding due to partial dislocation nucleation is also presented. The anisotropic elastic results for the KII load factor required for dislocation nucleation are shown to compare well with recently published molecular dynamics simulations of this process.

15. SUBJECT TERMS
anisotropic elasticity, dislocation nucleation, fracture, ductility

16. SECURITY CLASSIFICATION OF:			17. LIMITATION OF ABSTRACT	18. NUMBER OF PAGES	19a. NAME OF RESPONSIBLE PERSON
a. REPORT	b. ABSTRACT	c. THIS PAGE			19b. TELEPHONE NUMBER (*Include area code*)
Unclassified	Unclassified	Unclassified	UU	30	Lynn B. Munday 410-278-7511

Standard Form 298 (Rev. 8/98)
Prescribed by ANSI Std. Z39.18

Contents

List of Figures

List of Tables

Acknowledgments

Support is gratefully acknowledged from the U.S. Department of Defense (DOD) High-Performance Computing Modernization Office through the Multiscale Reactive Modeling of Insensitive Munitions Software Applications Institute. Computing support was provided by the DOD Supercomputing Resource Center located at the U.S. Army Research Laboratory.

1. Summary

This work reports anisotropic and isotropic elastic properties of dislocations and cracks in the α-phase of the energetic molecular crystal hexahydro-1,3,5-trinitro-s-triazine (αRDX). The properties determined in this work can be used to determine probable slip systems in αRDX and the structure of dislocations. The procedures given in this work for determination of the anisotropic dislocation line energy and crack tip dislocation nucleation load factors follow those outlined by Knap (*1*). This work contains a summary of the anisotropic elastic solutions for infinite straight dislocations given by Barnett and Swanger (*2*) and Barnett and Asaro (*3*) and the isotropic and anisotropic dislocation nucleation models of Rice (*4*) and Sun and Beltz (*5*). The appendix contains the Matlab implementation of the algorithms given in the text.

2. Elastic Constants

The orthotropic elastic constants used for αRDX are given in this section. The elastic constants are given in the material coordinates, X_i, which are aligned with the major axes of the material stiffness tensor. The linear elastic relationship between the stress and strain tensors, **σ** and **e**, are related by a fourth order tensor, C_{ijkl}. Voigt form uses major and minor symmetry of the stress and strain tensors to write the fourth-order tensor, C_{ijkl}, as a 6 × 6 matrix, c_{ij}. For an orthotropic material, the stress-strain relationship in Voigt form is given by

$$\boldsymbol{\sigma} = \mathbf{c} : \mathbf{e}$$

$$\begin{Bmatrix} \sigma_{11} \\ \sigma_{22} \\ \sigma_{33} \\ \sigma_{23} \\ \sigma_{31} \\ \sigma_{12} \end{Bmatrix} = \begin{bmatrix} c_{11} & c_{12} & c_{13} & 0 & 0 & 0 \\ c_{21} & c_{22} & c_{23} & 0 & 0 & 0 \\ c_{31} & c_{32} & c_{33} & 0 & 0 & 0 \\ 0 & 0 & 0 & c_{44} & 0 & 0 \\ 0 & 0 & 0 & 0 & c_{55} & 0 \\ 0 & 0 & 0 & 0 & 0 & c_{66} \end{bmatrix} \begin{Bmatrix} e_{11} \\ e_{22} \\ e_{33} \\ 2e_{23} \\ 2e_{31} \\ 2e_{12} \end{Bmatrix} \tag{1}$$

Previously reported (*6*, *7*) molecular dynamics simulations under an applied strain were used to determine the components of c_{ij}. Each volumetric strain component, e_{ii}, results in a triaxial state of stress, σ_{jj}, due to Poisson's effect and is used to determine the volumetric components of c_{ij}. Each shear strain results in a single linearly proportional shear stress, giving the shear components of c_{ij}. The compliance tensor, S_{ijkl}, is given by the inverse of the stiffness tensor, C_{ijkl}, but there is not a method available for taking the inverse of a fourth-order tensor and, due to material symmetries, the 81 components of C_{ijkl} would produce a rank deficient 9 × 9 matrix. The Voigt form of the stiffness tensor, c_{ij}, includes the crystal symmetries and therefore is not rank deficient and an inverse exists. The Voigt form of the compliance tensor, s_{ij}, given by the inverse of c_{ij}, in terms of common orthotropic engineering terms is given by

$$\mathbf{s} = \mathbf{c}^{-1} = \begin{bmatrix} 1/E_1 & -\nu_{21}/E_2 & -\nu_{31}/E_3 & 0 & 0 & 0 \\ -\nu_{12}/E_1 & 1/E_2 & -\nu_{32}/E_3 & 0 & 0 & 0 \\ -\nu_{13}/E_1 & -\nu_{23}/E_2 & 1/E_3 & 0 & 0 & 0 \\ 0 & 0 & 0 & 1/G_{23} & 0 & 0 \\ 0 & 0 & 0 & 0 & 1/G_{31} & 0 \\ 0 & 0 & 0 & 0 & 0 & 1/G_{12} \end{bmatrix} \quad (2)$$

where E_i is the orthotropic Young's modulus, ν_{ij} is the orthotropic Poisson's ratio and G_{ij} is the orthotropic shear modulus. Values for c_{ij}, s_{ij}, E_i, ν_{ij}, and G_{ij} are given in table 1.

Table 1. Orthotropic elastic and engineering constants for αRDX (*6*, *7*).

Stiffness Components (GPa)		**Compliance Components (GPa^{-1})**		**Engineering Constants (GPa)**	
c_{11}	25.0	s_{11}	0.0510	E_1	19.6
c_{22}	23.8	s_{22}	0.0561	E_2	17.8
c_{33}	23.4	s_{33}	0.0513	E_3	19.5
c_{44}	3.1	s_{44}	0.3226	G_{23}	3.1
c_{55}	5.2	s_{55}	0.1923	G_{31}	5.2
c_{66}	7.7	s_{66}	0.1299	G_{12}	7.7
c_{23}	8.8	s_{23}	–0.0148	ν_{21}	0.34
c_{31}	7.6	s_{31}	–0.0093	ν_{12}	0.38
c_{12}	10.6	s_{12}	–0.0193	ν_{31}	0.18
—	—	—	—	ν_{13}	0.18
—	—	—	—	ν_{32}	0.29
—	—	—	—	ν_{23}	0.26

Voigt and Reuss averages are used to find the isotropic bulk and shear modulii. The Voigt average assumes a uniform strain field leading to an overestimate of the stress field calculated from anistropic elasticity. The Reuss average assumes uniform stress and results in an underestimate of the stress field from anisotropic elasticity. The Voigt average for the bulk modulus, B_v, and shear modulus, G_v, found from the stiffness tensor are given by

$$B_V = \frac{1}{9}\sum_{i,j}^{3} C_{ij}$$
$$G_V = \frac{1}{15}(C_{11} + C_{22} + C_{33}) - \frac{1}{15}(C_{23} + C_{31} + C_{12}) + \frac{1}{5}(C_{44} + C_{55} + C_{66}) \quad (3)$$

and are tabulated in table 2 for αRDX. Likewise, the Reuss average for the bulk modulus, B_R, and shear modulus, G_R, found from the compliance tensor are given by

$$B_R = \left(\frac{1}{9} \sum_{i,j}^{3} S_{ij} \right)^{-1}$$
$$G_R = \left[\frac{4}{15}(S_{11} + S_{22} + S_{33}) - \frac{4}{15}(S_{23} + S_{31} + S_{12}) + \frac{1}{5}(S_{44} + S_{55} + S_{66}) \right]^{-1} \quad (4)$$

and are also tabulated in table 2 for αRDX. Table 2 also presents isotropic averages for the Young's modulus and Poisson ratio found for either Voigt or Reuss averages of the bulk and shear modulus using the following relationships

$$E = \frac{9BG}{3B + G}$$
$$\nu = \frac{3B - 2G}{2(3B + G)} \quad (5)$$

Table 2. Isotropic averages of orthotropic elastic constants for αRDX.

Voigt	**(GPa)**	**Reuss**	**(GPa)**
B_V	14.0	B_R	14.0
G_V	6.2	G_R	5.5
E_v	16.2	E_R	14.5
ν_v	0.31	ν_R	0.33

The elastic constants presented in table 1 are given in the laboratory or material coordinates, X_i, which are the coordinates where the stiffness and compliance tensors from equations 1 and 2 are in their simplest forms, showing the symmetry of the crystal. The material coordinates, X_i, are normally not coincident with the crack coordinates x_i as shown in figure 1. The crack coordinates shown in figure 1 are aligned so that the x_2 direction is normal to the crack face and the x_1 direction is aligned with the crack front. The dislocation geometry is also described in terms of these coordinates where the dislocation line direction of the dislocation to be emitted from the crack tip will be in the x_3 direction.

The anisotropic elasticity equations in the following sections were derived by Barnett and Swanger (*2*) to yield expressions that utilize the material coordinates. The equations also utilize the fourth order tensor version of the stiffness tensor, Cijkl. An algorithm for creating a fourth order tensor from the 6 × 6 Voigt form is given in the appendix.

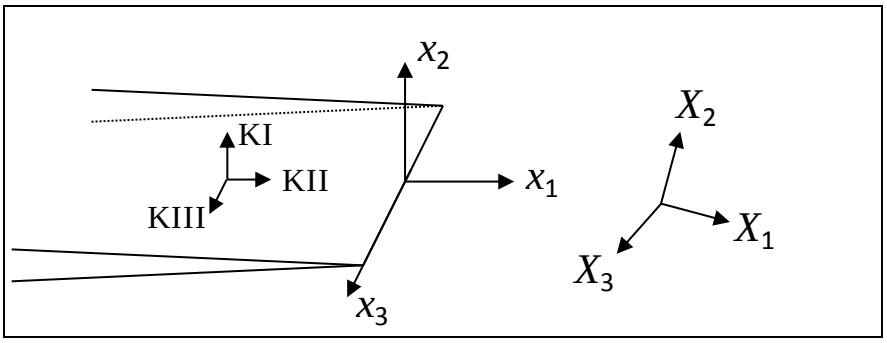

Figure 1. Coordinates used in elastic crack tip solution. X_i are the material coordinates aligning with the major axis of the material stiffness tensor, x_i are the crack tip coordinates, where x_1 is the direction of the crack front, x_2 is normal to the crack face, and x_3 is the plane dimension. K_I are the applied load intensity factors describing the local modes of deformation at the crack tip.

3. Anisotropic Elastic Dislocation Line Energy

This section will give a brief description of how to determine the dislocation line energy using the methodology developed by Barnett and Swanger (*2*). This section is a reproduction of their work and will therefore use the same constants and terminology. In their work they refer to the coordinates in which the elastic constants are defined in as the laboratory or material coordinates, X_i. In equation 1 of Barnett and Swanger (*2*), the energy per unit length of a dislocation line is given by

$$E = K_{mg} b_m b_g \ln\frac{R}{r_o} \quad \text{where } (m, g = 1,2,3) \tag{6}$$

where K_{mg}=K_{gm} is the energy prefactor that only depends on the elastic constants C_{ijkl} and the orientation of the dislocation with respect to the laboratory X_i coordinates. The other parameters in equation 6 are as follows **b** is the burgers vector, r_o is the radius of the dislocation core, R is a radial dimension on the same order as the specimen. In equation AI.1 of appendix I of Barnett and Asaro (*3*), a straightforward method for evaluating K_{mg} is given as

$$K_{mg} = \frac{1}{8\pi^2}\varepsilon_{pjw} t_j \left(C_{ngip} C_{wmrs} + C_{nmip} C_{wgrs}\right) \int_0^{\pi} z_s (dz_n/d\psi) M_{ir}^{-1} d\psi \tag{7}$$

where ε_{pjw} is the alternating or Levi-Cevita tensor, **t** is the dislocation line direction, **z** is any unit vector perpendicular to **t**, and ψ is an angular variable in the plane **z**•**t**=0 (see figure 2). M_{ir} is the symmetric Christoffel stiffness matrix given by $M_{ir} = C_{ijrs} z_j z_s$. M_{ir}^{-1} is the inverse of M_{ir}.

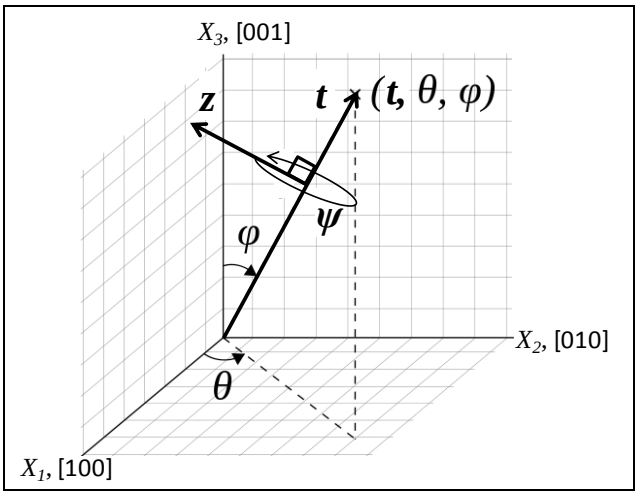

Figure 2. Spherical polar coordinates used to define the dislocation line direction, **t**, with respect to the crystal axes or laboratory axes, X_i. **z** is the unit normal vector to **t** and ψ is the angle of rotation integrated over in equation 7.

In our work, the dislocation line direction, **t**, with respect to the laboratory axis, X_i, is known a priori and is fixed. Using the spherical polar coordinates shown in figure 2, **t** is given by

$$t_m = \begin{Bmatrix} \sin\varphi\cos\theta \\ \sin\varphi\sin\theta \\ \cos\varphi \end{Bmatrix} \tag{8}$$

With **t** fixed, any unit vector **z** normal to **t** and its derivative are given by

$$\begin{aligned} z_m &= a_m\cos\psi + d_m\sin\psi \\ \frac{dz_m}{d\psi} &= -a_m\sin\psi + d_m\cos\psi \end{aligned} \tag{9}$$

where

$$a_m = \begin{Bmatrix} \sin\theta \\ \cos\theta \\ 0 \end{Bmatrix} \text{ and } d_m = \begin{Bmatrix} \cos\varphi\cos\theta \\ \cos\varphi\sin\theta \\ -\sin\varphi \end{Bmatrix} \tag{10}$$

The integral in equation 7 is evaluated using trapezoidal numerical integration yielding a fourth order tensor that is evaluated with the remaining terms of equation 7 yielding K_{mg}.

In table 3, values for the anisotropic prelogarithmic factor, $K_{mg}b_m b_g$, are given for several slip systems reported on by Munday (*7*), Munday et al. (*8*), and Mathew et al. (*9*). Isotropic values are also given using the Voigt and Reuss averages. The dislocation line energy prefactor for an isotropic material is given by

$$K_{iso} = \frac{G(1 - \nu \cos^2 \theta)}{4\pi(1 - \nu)} \tag{11}$$

where G and ν are the Voight or Reuss isotropic averages for the shear modulus and Poisson's ratio, respectively, and θ is the angle between the line direction, ***t***, and Burger's vector, ***b***. Plots of the prelogarithmic energy factors as a function θ are shown in figure 3 for ***b*** = ½[100] dislocations on the (010) or (001) glide planes. Matlab algorithms for determining the line energies are given in the appendix.

Table 3. Anisotropic and isotropic prelogarithmic energy factor ($E = K_{mg} b_m b_g$) for αRDX slip systems.

Slip plane, **n**	Burgers vector, **b**	Line direction, **t**	Dislocation type	E Aniso (J m^{-1})e-9	E Voigt (J m^{-1})e-9	E Reuss (J m^{-1})e-9
(010)	½[100]	[001]	edge	0.37	0.32	0.28
(010)	½[100]	[100]	screw	0.22	0.22	0.19
(010)	[001]	[100]	edge	0.62	0.76	0.69
(010)	[001]	[001]	screw	0.34	0.53	0.47
(001)	[010]	[010]	screw	0.5	0.64	0.56
(001)	½[100]	[100]	screw	0.22	0.22	0.19
(001)	½[100]	[010]	edge	0.33	0.32	0.28
(001)	½[010]	[100]	edge	0.19	0.23	0.21
(021)	½[0$\bar{1}$2]	[0$\bar{1}$2]	screw	0.64	0.69	0.61
(021)	[0$\bar{1}$2]	[0$\bar{1}$2]	screw	2.56	2.75	2.42
(021)	½[100]	[012]	edge	0.36	0.32	0.29
(021)	½[100]	[100]	screw	0.22	0.22	0.19
(021)	[100]	[100]	screw	0.9	0.88	0.78
(011)	[100]	[100]	screw	0.9	0.88	0.78
(011)	[100]	[100]	edge	1.37	1.27	1.16
(011)	[0$\bar{1}$1]	[0$\bar{1}$1]	screw	1.28	1.17	1.03

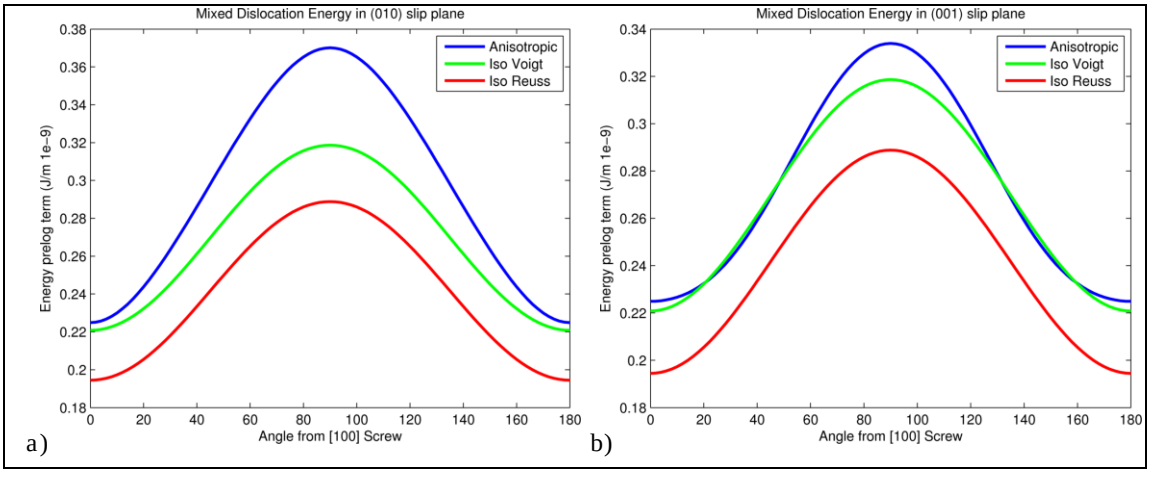

Figure 3. Anisotropic and isotropic energy prelog factors as a function of dislocation type for dislocations with **b** = ½[1 0 0] on the (a) (010) and (b) (001) glide planes.

4. Anisotropic Dislocation Nucleation

A summary of the anisotropic version of Rice's (*4*) dislocation nucleation continuum model developed by Sun and Beltz (*5*) will be presented followed by simplifications made for the systems under pure mode II or mode III loading. In this work, the dislocation line direction, ***t***, given in equation 8 and shown in figure 2 coincides with the crack front, given as the x_3-coordinate in figure 4.

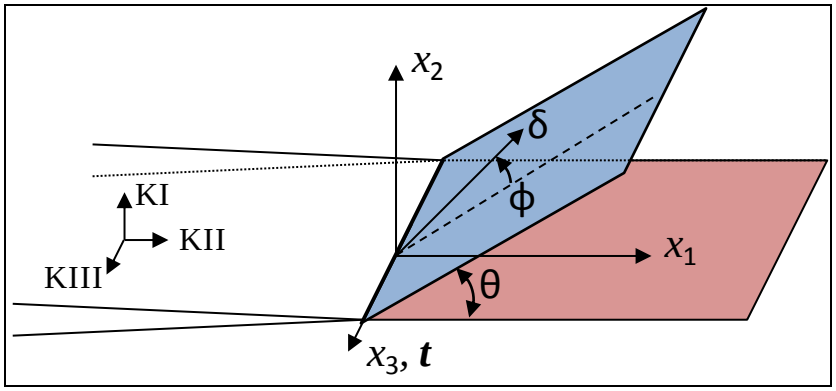

Figure 4. Crack tip geometry where the red plane is coincident with the crack plane, the crack front coincides with the x_3-coordinate and the dislocation line direction, ***t***, and the slip plane is shown in blue and is tilted by an angle θ relative to the crack plane. The slip direction is given by δ and angle ϕ.

In equation 58 of Barnett and Asaro (*3*), the Griffith energy for a loaded crack tip in an anisotropic material is

$$G = \frac{1}{8\pi} k_m K_{mg}^{-1} k_g \tag{12}$$

where K_{mg} is the anisotropic energy prefactor given by equation 7, and k_m = (K1,K2,K3) = (KII,KI,KIII) are the applied stress intensity factors as shown in figure 4. In fracture mechanics, equation 12 is normally given as

$$G = k_m \Lambda_{\mathrm{mg}} k_g \tag{13}$$

where $\Lambda_{\mathrm{mg}} = K_{mg}^{-1}/8\pi$. K_{mg} and Λ_{mg} are symmetric and can have off-diagonal elements.

Sun and Beltz (*5*) give the modified dislocation nucleation criterion of Rice (*4*) for an anisotropic media as

$$s_m(\phi) k_m^{eff} = \sqrt{\gamma_{us} p(\phi, \theta)} \tag{14}$$

where $s_m(\phi)$ = [cos ϕ, 0, sin ϕ] is the orientation of the slip direction δ on the slip plane and γ_{us} is the unstable stacking fault energy found from the generalized stacking fault energy surface. k_m^{eff} is the effective stress intensity factor on the slip plane tilted at an angle of θ relative to the crack plane and is given by Rice (*4*) as

$$k_m^{eff} = F_{mg}(\theta)k_g = \begin{bmatrix} \cos\frac{\theta}{2}\left[1-3\sin^2\frac{\theta}{2}\right] & \cos^2\frac{\theta}{2}\sin\frac{\theta}{2} & 0 \\ -3\cos^2\frac{\theta}{2}\sin\frac{\theta}{2} & \cos^3\frac{\theta}{2} & 0 \\ 0 & 0 & \cos\frac{\theta}{2} \end{bmatrix} k_g \tag{15}$$

Sun and Beltz (*5*) point out that the term $s_m k_m^{eff}$ is the effective stress intensity factor due to the combination of KII and KIII loading along the s_m direction of the slip plane.

The function $p(\phi,\theta)$ describes the effective material properties in the direction of slip and is given by

$$p(\phi,\theta) = 8\pi s_m K_{mg}^{(\theta)} s_g \tag{16}$$

where $8\pi K_{mg}$ from equation 12 is used instead of Λ_{mg}. $K_{mg}^{(\theta)}$ is related to K_{mg} given in equation 7 by the rotation from the laboratory coordinates, X_i, to the crack coordinates, x_i, in figure 4, given by

$$K_{mg}^{(\theta)} = R_{mi}K_{ij}R_{jg} \tag{17}$$

The rotation matrix, R_{ij}, rotating K_{mg} to the crack coordinates, x_i, by θ about the x_3 axis is

$$R_{ij} = \begin{bmatrix} \cos\theta & \sin\theta & 0 \\ -\sin\theta & \cos\theta & 0 \\ 0 & 0 & 1 \end{bmatrix} \tag{18}$$

In this work, the crack tip geometry is simplified as shown in figure 5, where the slip plane is coincident with the crack plane, θ = 0. The rotation matrix given by equation 18 is equal to the identity and equation 17 simplifies to $K_{ij}^{(\theta)} = K_{ij}$. For the emission of a pure edge dislocation, the slip direction, δ, coincides with the x_1 or *KII* direction, where ϕ = 0 and $s_m(0)$ = [100], and equation 16 simplifies to $p(0,0) = 8\pi K_{11}$. The stress intensity factors for this configuration given by equation 14 are

$$KII = \sqrt{8\pi K_{11}\gamma_{us}} \tag{19}$$

where the K_{mg} tensor with component K_{11} is found from equation 7 for **t** = [KII 0 0] and γ_{us} is the energy barrier to slip in the δ direction.

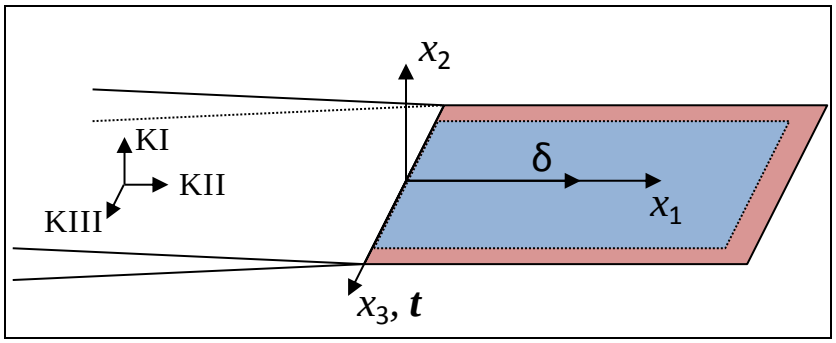

Figure 5. Simplified crack tip geometry for the emission of a pure edge dislocation where the blue slip plane is coincident with the red crack plane (θ = 0) and the slip direction, δ, is aligned with the KII direction (ϕ = 0).

Alternatively, for the emission of a pure screw dislocation shown in figure 6, the slip direction, δ, coincides with the x_3 or *KIII* direction where ϕ = π/2, $s_m(\pi/2)$ = [001], and equation 16 simplifies to $p(\pi/2,0) = 8\pi K_{33}$. The stress intensity factors for this configuration is given by equation 14 is

$$KIII = \sqrt{8\pi K_{33}\gamma_{us}} \tag{20}$$

where K_{33} component now to a K_{mg} tensor given by equation 7 for **t** = [0 0 KIII] and γ_{us} is the energy barrier to slip in the δ direction. Stress intensity factors for isotropic averaged material properties are given by substituting in equations 19 or 20 values for *K* determined from equation 11.

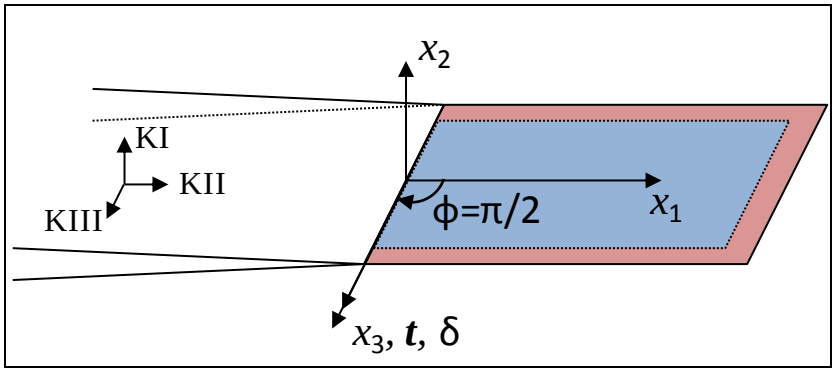

Figure 6. Simplified crack tip geometry for the emission of a pure screw dislocation where the blue slip plane is coincident with the red crack plane (θ = 0) and the slip direction, δ, is aligned with the KIII direction (ϕ = π/2).

Generalized stacking fault (GSF) energy surfaces for two αRDX slip systems are shown in figure 7 for the (010) slip plane (*7*, *8*). These GSF surfaces provide energy barriers, γ_{us}, for a crack tip geometry with an $\boldsymbol{x_2}$ = [010] crack face and $\boldsymbol{x_3}$ = **t**=[001] or [100] crack front /dislocation line direction. Anisotropic and isotropic critical stress intensity factors for these crack tip geometries from equations 19 and 20 are given in table 4 along with values for K_{mg} from equation 7 and 11. Using anisotropic material properties, the lowest nucleation threshold for the (010) crack face is a screw type ½[100] dislocation emitted under *KIII* loading. This slip system also had the lowest dislocation line energy in table 3.

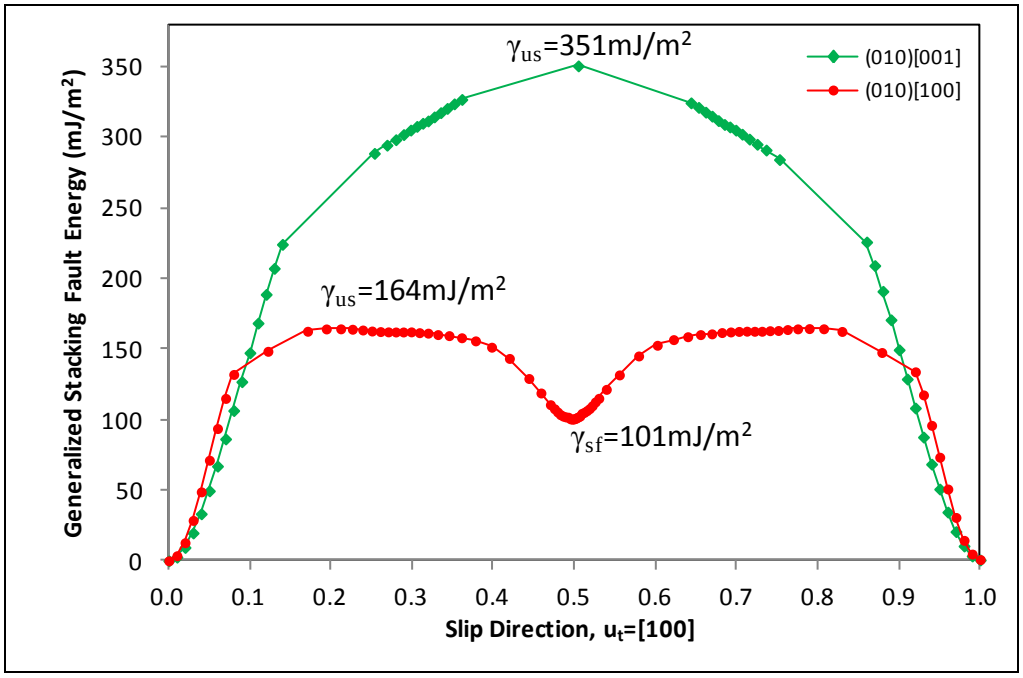

Figure 7. GSF energy surfaces for dislocations on the (010) slip plane.

Table 4. Anisotropic and isotorpic critical stress intensity factors for the (010) crack face in αRDX.

Slip plane	δ	***t***, line dir	Dislocation Type / Load	γ_{us} (mJ/m^{-2})	K_{mg} (MJ/m)			Critical *KII* or *KIII* (Mpa m^{½})		
					Aniso	Voigt	Reuss	Aniso	Voigt	Reuss
(010)	[100]	[001]	edge / KII	164	826	714	647	0.058	0.054	0.052
(010)	[001]	[001]	screw / KIII	351	320	495	436	0.053	0.045	0.042
(010)	[100]	[100]	screw / KIII	164	576	495	436	0.049	0.066	0.062
(010)	[001]	[100]	edge / KII	351	503	714	647	0.067	0.079	0.076

The (010)[100] GSF surface in figure 7 has a local energy minimum indicating a stable stacking fault configuration for this slip system. In the case of dislocation nucleation, a stable stacking fault means a partial dislocation will be emitted from the crack tip. The shear stress at the crack front will cause the partial dislocation to move away from tip, leaving behind a stacking fault. The stacking fault material is at a higher energy pulling the partial dislocation back toward the

crack tip. There is also an image force pulling the partial dislocation back toward the crack tip. A stable equilibrium position, r_A, for the partial dislocation is found when the Peach Koehler forces due to the externally loaded crack tip are balanced out by the stacking fault and image forces, leading to equation 22 in Sun and Beltz (*5*) and reproduced here to include lattice frictional forces

$$\frac{k_A b_A}{\sqrt{2\pi r_A}} - \left(\gamma_{sf} + \sigma_p b_A\right) - \frac{b_A^2 p(\phi_A)}{8\pi r_A} = 0 \tag{21}$$

where k_A is the applied stress intensity factor, b_A is the Burgers vector of the partial dislocation being emitted, $p(\phi_A)$ is from equation 16, and $\sigma_p b_A$ is the friction force due to lattice resistance where σ_p is the Peierls stress. For the edge-type partial dislocations described in table 4, $k_a = KII$ and $\phi_A = 0$, leading to

$$\frac{KII\, b_A}{\sqrt{2\pi r_A}} - \left(\gamma_{sf} + \sigma_p b_A\right) - \frac{b_A^2 8\pi K_{11}}{r_A} = 0 \tag{22}$$

The equilibrium position, r_a, is found using equation 24 in Sun and Beltz, reproduced here for the edge-type partial dislocations

$$r_A = 8\pi \left\{ \frac{b_A K_{11}}{KII\left[1 - \sqrt{1 - \left(\frac{KII}{KII_{Aniso}}\right)^2 \left(\frac{\gamma_{sf} + \sigma_p b_A}{\gamma_{us}}\right)}\right]} \right\}^2 \tag{23}$$

where *KII* is the load being applied, KII_{Aniso} is the critical anisotropic load factor calculated for emission of the partial dislocation and $KII > KII_{Aniso}$, meaning the partial has been nucleated. The isotropic version of equation 23 is given by equation 38 in Rice (*4*) and reproduced here for an edge dislocation with the addition of lattice friction

$$r_{iso} = \frac{\left(\frac{KII}{KII_{crit}}\right)^2 \left(\frac{G b_A^2}{\gamma_{us}}\right)}{4\pi(1-\upsilon)\left[1 - \sqrt{1 - \left(\frac{KII}{KII_{iso}}\right)^2 \left(\frac{\gamma_{sf} + \sigma_p b_A}{\gamma_{us}}\right)}\right]^2} \tag{24}$$

where KII_{Aniso} is the isotropic load factor calculated for emission of the partial dislocation. Lattice friction is usually not included for most materials because the Peierls stress, σ_p, is usually on the order of 10^{-4} to $10^{-2}G$. The lattice friction cannot be ignored for aRDX because the Burger's vectors are large and Mathew et al. (*9*) found σ_p to be approximately 3%–10% of *G*. The large lattice friction could be due to steric interactions. Values for r_A and r_{iso} for the (010)½[100] slip system are given in table 5 for both with and without lattice friction. For cases

with lattice friction, alternative values for σ_p are presented. The "Iso Fit" and "Aniso Fit" σ_p values were found by fitting to *r* from the simulation data for KII = 0.07 MPa $m^{½}$. The MD and GSF σ_p values were found by Mathew et al. (*9*) using molecular dynamics and the Peierls Nabarro model with the GSF data from Munday (*8*) and shown in figure 7. Including σ_p in equations 23 and 24 produces imaginary numbers for several values of *KII*. The values produced by the molecular dynamics simulations (*10*) of a crack tip given in the "Sim." column of table 5 do not match any of the σ_p values over the range of *KII* loads.

Table 5. Location of the first (010)½[100] partial edge dislocation emitted from the crack tip for the anisotropic and isotropic models. Each row corresponds to the σ_p value given at the top of the table. The "Sim." shows values from a molecular dynamics simulation (*10*).

		σ_p (GPa)					
		ISOTROPIC MODEL		ANISOTROPIC MODEL			
			Iso Fit		Aniso Fit	GSF	MD
		None	130	None	115	201	232
KII (Mpa $m^{½}$)	Sim. (Å)	r_{iso}(Å)	r_{iso}(Å)	r_A(Å)	r_A(Å)	r_A(Å)	r_A(Å)
0.054		135	NaN	NaN	NaN	NaN	NaN
0.058		175	25	156	NaN	NaN	NaN
0.060		189	31	170	NaN	NaN	NaN
0.065		235	47	215	44	NaN	NaN
0.070	62	284	63	263	62	17	NaN
0.075		336	79	315	80	34	23
0.080		392	95	369	98	45	35
0.085		452	113	427	117	57	45
0.090	76	514	131	489	137	69	55

After the partial dislocation is nucleated the material at the crack tip is in the stacking fault configuration. The increased energy of the stacking fault configuration lowers the energy barrier for emission of the second partial dislocation. For the case where the partial dislocation's Burgers vectors are in the same direction as the full dislocation, the first partial dislocation completely shields the crack tip from the k_{crit} load at which it was emitted. For the edge dislocation, the load for emission of the second partial dislocation is then reduced to

$$KII = \sqrt{8\pi K_{11}\left(\gamma_{us} - \gamma_{sf}\right)} \tag{25}$$

Values for critical KII loads for emission of the first and second partial dislocation are given in table 6 for several slip systems that were determined by Munday et al. (*8*) to produce partial dislocations in αRDX.

Table 6. Anisotropic and isotropic critical stress intensity factors for the (010) crack face in αRDX. Unstable stacking fault energy, γ_{us}, given by Munday et al. (*8*).

Slip plane, **n**	Burgers vector, **b**	Line direction, **t**	Type	γ_{us} (mJ m^{-2})	KII Aniso		KII Voigt		KII Reuss	
					1st	2nd	1st	2nd	1st	2nd
(010)	½[100]	[001]	edge	164	0.058	0.036	0.054	0.034	0.052	0.032
(001)	½[100]	[010]	edge	260	0.070	0.032	0.068	0.031	0.065	0.030
(011)	½[100]	[011]	edge	255	0.070	0.047	0.068	0.045	0.064	0.043
(021)	½[100]	[012]	edge	250	0.071	0.036	0.067	0.034	0.064	0.032

After the second partial dislocation is emitted, the two partial dislocations remain separated by the stacking fault. Even in the absence of a defect, it is energetically favorable for a full dislocation to dissosciate into two partials with a fractional Burgers vector separated by a stacking fault because the dislocation line energy given by equation 6 is proportional to $|b|^2$. In the bulk crystal the partial dislocations are pushed apart by elastic forces due to both partial dislocations having similar Burger's vectors. As the partial dislocations move away from one another they increase the size of the stacking fault resulting in an attractive force holding them together. An equilibrium configuration is reached where the two forces are balanced and are described in equations 10-14 and 13-150 of Hirth and Lothe (*11*). For the pure edge-type partial dislocations given in table 6, the equilibrium equation from Hirth and Lothe is simplified as

$$r_a = \frac{2K_{mg}b_m b_g}{\gamma_{sf}} \tag{26}$$

Values for r_a are given in table 7 for anisotropic and isotropic K_{mg} values.

Table 7. Anisotropic and isotorpic partial dislocation separation distances for **b** = ½[100] edge-type dislocations.

Slip plane, **n**	Burgers vector, **b**	Line direction, **t**	Dislocation type	γ_{sf} (mJ m^{-2})	r_a (Å)		
					Aniso	Voigt	Reuss
(010)	½[100]	[001]	edge	101	73	63	65
(001)	½[100]	[010]	edge	206	32	31	32
(011)	½[100]	[011]	edge	140	49	46	47
(021)	½[100]	[012]	edge	187	38	34	35

5. Conclusion

Several dislocation and crack tip properties were presented in this work that are useful for energetically ranking slip system activity and predicting the dislocation structure. Both isotropic and anisotropic results were provided and the isotropic results are shown to predict dislocation nucleation at smaller thresholds than the anisotropic model. The isotropic and anisotropic models provided the same energetic ranking based on dislocation line direction. For isotropic materials, the line energy of a screw dislocation is always lower than that of edge dislocations due to edge dislocations being scaled by $(1-\upsilon)^{-1}$ but for anisotropic materials this is not always the case, see for instance NiAl (*12*) and aFe (*13*). However, for the slip systems we studied in this work, the anisotropic line energy for screw dislocations was always lower than edge dislocations and was in general agreement with the isotropic model.

6. References

1. Knap, J. *Surface Stress Effects on Dislocation Nucleation Processes*, Mechanical Engineering, PhD Dissertation: Arizona State University, 1997.
2. Barnett, D. M.; Swanger, L. A. *The Elastic Energy of a Straight Dislocation in an Infinite Anisotropic Elastic Medium. Physica Status Solidi b* **1971**, *48* (1), 419–428.
3. Barnett, D. M.; Asaro, R. J. The Fracture Mechanics of Slit-like Cracks in Anisotropic Elastic Media. *J. Mech. and Phys. of Solids* **1972**, *20*, 353–366.
4. Rice, J. R. Dislocation Nucleation From a Cracktip: An Analysis Based on Teh Peierls Concept. *J. Mech. and Phys. of Solids* **1992**, *40* (2), 239–271.
5. Sun, Y.; Beltz, G. E. Dislocation Nucleation From a Crack Tip: A Formulation Based on Anisotropic Elasticity. *J. Mech. and Phys. of Solids* **1994**, *42* (12), 1905–1932.
6. Munday, L. B., et al. Simulations of High-Pressure Phases in RDX. *The Journal of Physical Chemistry B* **2011**, *115*, 4378–4386.
7. Munday, L. B. *Computational Study of the Structure and Mechanical Properties of the Molecular Crystal RDX*. Mechanical Engineering, PhD Dissertation,University of Maryland: College Park, MD, 2011.
8. Munday, L. B.; Solares, S. D.; Chung, P. W. Generalized Stacking Fault Energy Surfaces in the Molecular Crystal αRDX. *Philosophical Magazine* **2012**, *92* (24), 3036–3050.
9. Mathew, N.; Picu, C. R.; Chung, P. W. Peierls Stress of Dislocations in Molecular Crystal Cyclotrimethylene Trinitramine. *J. Phys. Chem. A* **2013**, *117*, 5326–5334.
10. Munday, L.B.; Mitchell, R.L.; Knap, J.; Chung, P.W., Role of molecule flexibility on the nucleation of dislocations in molecular crystals. *App. Phys. Lett.* **2013**, *103*, 151911.
11. Hirth, J. P.; Lothe, J. *Theory of Dislocations.* Wiley: New York, NY, 1992.
12. Sih, G. C.; Paris, P. C.; Irwin, G. R. On Cracks in Rectilinearly Anisotropic Bodies. *Int. J. of Fracture* **1965**, *1*, (3), 189–203.
13. Suo, Z. Delamination Specimens for Orthotropic Materials. *J. App. Mech.* **1990**, *57*, 627–634.

INTENTIONALLY LEFT BLANK.

Appendix. Matlab Code for Dislocation Line Energies and Nucleation

This appendix appears in its original form, without editorial change.

```
% Determine Anistropic and isotropic dislocation line energy and
% dislocation nucleation form a crack tip.
%
% This script provides the data for the Anisotropic dislocation line energy
% and crack tip dislocation nucleation ARL technical report. Equation
% numbers given in this script correspond to equation numbers given in the
% report.
%
% Anistropic dislocation orientation prefactor tensor determined from
% equations given by Barnett & Swanger (PhysStat.Sol 1971) and Barnett &
% Asaro (JMPS 1972).
%
% KII isotropic and anisotropic crack tip loading factors for dislocation
% nucleation using in Rice's (JMPS 1994) isotropic dislocation nucleation
% model or Sun & Beltz's (JMPS 1994) anisotropic dislocation nucleation
% model.
%
% Lynn Munday, August 2012
%
close all hidden,clear all, clc
format short

%------MANUAL INPUT-----------------------------------------------------------
%
% RDX stable and unstable stacking energy J/m^2=Pa*m
% From Munday thesis (UMd 2011) and Munday et al. (Phil Mag 2012)
y_us=164e-3;  % for (010)[100]
y_sf=101e-3;

% y_us=260e-3;  % for (001)[100]
% y_sf=206e-3;
%
% y_us=255e-3;  % for (011)[100]
% y_sf=140e-3;
%
% y_us=250e-3;  % for (021)[100]
% y_sf=187e-3;

%lattice vectors a,b,c or [100][010][001]
latVec=[13.366      0      0;...
           0   11.334      0;...
           0        0 10.341]*1e-10;

bvec_n=0.5*[1 0 0];    %unit burgers vector / slip direction
line_dir=[0 0 1];      %disocation line direction
bvec=latVec*bvec_n';   %burgers vector


% RDX properties (MPa) Table 3.6, p79 of Munday thesis (UMd 2011) and
% Munday et al. (JPCB 2010)
% Voigt Stiffness Coefficients from Munday Dissertation
C11=25e3;
C22=23.8e3;
C33=23.4e3;
C44=3.1e3;
C55=5.2e3;
C66=7.7e3;
C23=8.8e3;
C13=7.6e3;
C12=10.6e3;
```

```
%--------END MANUAL INPUT-----------------------------------------------------
% Voight notation
Cv=[C11 C12 C13   0   0   0;...
    C12 C22 C23   0   0   0;...
    C13 C23 C33   0   0   0;...
      0   0   0 C44   0   0;...
      0   0   0   0 C55   0;...
      0   0   0   0   0 C66];
S=inv(Cv);
% Find average isotropic material Properties
% Voigt Average - uniform strain, over-estimate of stresses (Get from C)
% bulk modulus
Bv=0;
for i=1:3
  Bv=Bv+sum(Cv(i,1:3));
end
Bv=Bv/9;
% shear modulus
Gv=(Cv(1,1)+Cv(2,2)+Cv(3,3))/15-
(Cv(1,2)+Cv(2,3)+Cv(1,3))/15+(Cv(4,4)+Cv(5,5)+Cv(6,6))/5;
% Youngs Modulus & Poissons Ratio
Ev=(9*Bv*Gv)/(3*Bv+Gv);
nuv=(3*Bv-2*Gv)/2/(3*Bv+Gv);
% Reuss Average - uniform stres, under-estimate of stressses (Get from S)
Br=0;
for i=1:3
  Br=Br+sum(S(i,1:3));
end
Br=1/Br;
% Shear Modulus
Gr=4/15*(S(1,1)+S(2,2)+S(3,3))-4/15*(S(1,2)+S(2,3)+S(1,3))+1/5*(S(4,4)+S(5,5)+S(6,6));
Gr=1/Gr;
% Youngs Modulus & Poissons Ratio
Er=(9*Br*Gr)/(3*Br+Gr);
nur=(3*Br-2*Gr)/2/(3*Br+Gr);

fprintf('\n\nISOTROPIC PROPERTIES:\n')
fprintf(' Voigt Avg Properties: Ev=%6.2f, nuv=%6.2f, Gv=%6.2f , Bv=%6.2f
\n',Ev,nuv,Gv,Bv)
fprintf(' Reuss Avg Properties: Er=%6.2f, nur=%6.2f, Gr=%6.2f , Br=%6.2f
\n',Er,nur,Gr,Br)

%-------------------------------------------------------------------------------
% get fourth order C
C=zeros(3,3,3,3);
for i=1:3
  for j=1:3
    for k=1:3
      for l=1:3
        m=0;
        n=0;
        if i==j
          m=i;
        elseif ((i==2 && j==3)||(i==3 && j==2))
          m=4;
        elseif ((i==1 && j==3)||(i==3 && j==1))
          m=5;
        elseif ((i==1 && j==2)||(i==2 && j==1))
          m=6;
        end
        if k==l
          n=l;
        elseif ((k==2 && l==3)||(k==3 && l==2))
```

```
          n=4;
        elseif ((k==1 && l==3)||(k==3 && l==1))
          n=5;
        elseif ((k==1 && l==2)||(k==2 && l==1))
          n=6;
        end
        C(i,j,k,l)=Cv(m,n);
      end
    end
  end
end

%----CALCULATE KK-------------------------------------------------------------
%permutation or Levi-Cevita 3x3x3 tensor (using linear indexing of matrix)
lc = zeros(3,3,3);
lc([8 12 22]) = 1;
lc([6 16 20]) = -1;

%  Integral for equation 2.2
t=line_dir/norm(line_dir); %disocation line direction -- eq 2.3
r=norm(t);
theta=atan2(t(2),t(1));
phi=acos(t(3)/r);
a=[sin(theta) -cos(theta) 0]; %eq 2.5
d=[cos(phi)*cos(theta) cos(phi)*sin(theta) -sin(phi)]; % eq 2.5

%Integral Range: psi ranges 0 to pi
psi_1=0;
psi_2=pi;
Ninc=200;  % # of midpoint summation intervals
psi_inc=(psi_2-psi_1)/Ninc;
intzM=zeros(3,3,3,3);
intzMiso=zeros(3,3,3,3);
LAM3=zeros(3,3);
for inc=1:Ninc  %midpoint integration loop for intgral of christophel matrix
  psi=psi_1+(inc-1)*psi_inc;
  z(1:3) =a*cos(psi)+d*sin(psi);  %eq 2.4
  dz(1:3)=-a*sin(psi)+d*cos(psi);  %eq 2.4

  % Christoffel stiffness -- C_ijrs z_r z_s
  M=zeros(3,3);
  for i=1:3
    for r=1:3
      for j=1:3
        for s=1:3
          M(i,r)=M(i,r)+C(i,j,r,s)*z(j)*z(s);
        end
      end
    end
  end

  %midpoint integration of Christophel terms for eq 2.2
  invM=inv(M);
  for s=1:3
    for n=1:3
      for i=1:3
        for r=1:3
          intzM(s,n,i,r)=intzM(s,n,i,r) + (z(s)*dz(n)*invM(i,r))*psi_inc;
        end
      end
    end
  end
```

```
end

% SOLVE FOR ANISOTROPIC DISLOCATION COMPLIANCE OR ORIENTATION PREFACTOR TENSORS
% this is the inverse of LAMBDA given by Sun & Beltz (JMPS 1994) etc.
KK_BA=zeros(3,3);  % Barnett & Asaro JMPS v.20 1972
for m=1:3
  for g=1:3
    for p=1:3
      for j=1:3
        for w=1:3
          for n=1:3
            for i=1:3
              for r=1:3
                for s=1:3
                  % -- Equation 2.2
                  KK_BA(m,g)=KK_BA(m,g)+1/8/pi^2*lc(p,j,w)*t(j)...
                           *(C(n,g,i,p)*C(w,m,r,s)+C(n,m,i,p)*C(w,g,r,s))...
                           *intzM(s,n,i,r);
                end
              end
            end
          end
        end
      end
    end
  end
end

%%%%---OUTPUT RESULTS---

%
% Dislocation energy
Eaniso=bvec'*(KK_BA)*bvec * 1e6 * 1e9; % eq 2.1
cos_theta=dot(bvec,line_dir/norm(line_dir))/norm(bvec);
Eiso_v=1/4/pi*Gv*(1-nuv*cos_theta^2)/(1-nuv)*(norm(bvec))^2*1e6*1e9;%eq 2.6
Eiso_r=1/4/pi*Gr*(1-nur*cos_theta^2)/(1-nur)*(norm(bvec))^2*1e6*1e9;
fprintf('\n\nENERGY PRELOG FACTOR (Jm^-1*1e-9): \n\n')
fprintf(' Anisotropic     = %-6g\n',Eaniso)
fprintf(' Isotropic Voigt = %-6g\n',Eiso_v)
fprintf(' Isotropic Reuss = %-6g\n',Eiso_r)

%
% splitting distance between two edge partials
d_aniso=(4*pi*bvec'*(KK_BA)*bvec) /2/pi/(y_sf*1e-6)*1e10; %eq 3.17
d_isov= (Gv/(1-nuv))/2/pi/(y_sf*1e-6)*(norm(bvec))^2*1e10;
d_isor= (Gv/(1-nur))/2/pi/(y_sf*1e-6)*(norm(bvec))^2*1e10;
fprintf('\n\nEDGE PARTIAL SPLITTING DISTANCE (A): \n\n')
fprintf(' Anisotropic     = %-6g\n',d_aniso)
fprintf(' Isotropic Voigt = %-6g\n',d_isov)
fprintf(' Isotropic Reuss = %-6g\n',d_isor)
%
% NUCLEATION FOR KII LOADING FOR EMISSION OF EDGE DISLOCATION
% equation 3.8
fprintf('\n\n KII LOAD FACOTRS FOR FIRST PARTIALS (MPa sqrt(m)): \n\n')
fprintf(' Isotropic Voigt = %-6g\n',sqrt(2*Gv/(1-nuv)*y_us*1e-6)) %eq
fprintf(' Isotropic Reuss = %-6g\n',sqrt(2*Gr/(1-nur)*y_us*1e-6))
fprintf(' Anisotropic     = %-6g\n',sqrt(8*pi*KK_BA(1,1)*y_us*1e-6))

% equation 3.21
fprintf('\n\n KII LOAD FACOTRS FOR SECOND PARTIAL: \n\n')
fprintf(' Isotropic Voigt = %-6g\n',sqrt(2*Gv/(1-nuv)*(y_us-y_sf)*1e-6))
fprintf(' Isotropic Reuss = %-6g\n',sqrt(2*Gr/(1-nur)*(y_us-y_sf)*1e-6))
fprintf(' Anisotropic     = %-6g\n',sqrt(8*pi*KK_BA(1,1)*(y_us-y_sf)*1e-6))
```

NO. OF COPIES	ORGANIZATION
1 (PDF)	DEFENSE TECHNICAL INFORMATION CTR DTIC OCA
1 (PDF)	DIRECTOR US ARMY RESEARCH LAB IMAL HRA
1 (PDF)	DIRECTOR US ARMY RESEARCH LAB RDRL CIO LL
1 (PDF)	GOVT PRINTG OFC A MALHOTRA
3 (PDF)	RDRL CIH C J KNAP L MUNDAY RDRL WML B E BYRD